Mechanochemical Synthesis of Pharmaceutical Cocrystal Suspensions via Hot Melt Extrusion: Enhancing Cocrystal Yield

Li, S., Yu, T., Tian, Y., Lagan, C., Jones, D., & Andrews, G. (2017). Mechanochemical Synthesis of Pharmaceutical Cocrystal Suspensions via Hot Melt Extrusion: Enhancing Cocrystal Yield. *Molecular Pharmaceutics*, *15*(9), 3741-3754. https://doi.org/10.1021/acs.molpharmaceut.7b00979

Published in:
Molecular Pharmaceutics

Document Version:
Peer reviewed version

Article

Mechanochemical Synthesis of Pharmaceutical Cocrystal Suspensions via Hot Melt Extrusion: Enhancing Cocrystal Yield

Shu Li, Tao Yu, Yiwei Tian, Colette Lagan, David S. Jones, and Gavin P. Andrews

Mol. Pharmaceutics, **Just Accepted Manuscript** • DOI: 10.1021/acs.molpharmaceut.7b00979 • Publication Date (Web): 22 Nov 2017

Mechanochemical Synthesis of Pharmaceutical Cocrystal Suspensions via Hot Melt Extrusion: Enhancing Cocrystal Yield

Shu Li, Tao Yu, Yiwei Tian, Colette Lagan, David S. Jones, and Gavin P. Andrews*,

Pharmaceutical Engineering Group, School of Pharmacy, Medical Biology Centre, Queen's University, Belfast BT9, Northern Ireland.

Correspondence to: Gavin P. Andrews

(Telephone: +44-28-9097-2646; E-mail: g.andrews@qub.ac.uk)

Running Title: Cocrystals via Mechanochemical synthesis

Key words: Cocrystal suspension, mechanochemical synthesis, Flory-Huggins phase diagrams, solubility parameter, hot melt extrusion, yield.

Abstract

Pharmaceutical cocrystals have attracted increasing attention over the past decade as an alternative way to modify the physicochemical properties and hence improve the bioavailability of a drug, without sacrificing thermodynamic stability. Our previous work has demonstrated the viability of *in-situ* formation of ibuprofen/isonicotinamide cocrystal suspensions within a matrix carrier via a single-step hot-melt extrusion (HME) process. The key aim of the current work is to establish optimised processing conditions to improve cocrystal yield within extruded matrices.

The solubility of each individual cocrystal component in the matrix carrier was estimated using two different methods, calculation of Hansen solubility parameters, and Flory-Huggins solution theory using melting point depression measurement, respectively. The latter was found to be more relevant to extrusion cocrystallisation because of the ability to predict miscibility across a range of temperatures. The predictions obtained from the F-H phase diagrams were verified using ternary extrusion processing. Temperatures that promote solubilisation of the parent reagents during processing, and precipitation of the newly formed cocrystal were found to be the most suitable in generating high cocrystal yields. The incorporation of intensive mixing/kneading elements to the screw configuration was also shown to significantly improve the cocrystal yield when utilising a matrix platform. This work has shown that intensive mixing in combination with appropriate temperature selection, can significantly improve the cocrystal yield within a stable and low viscosity carrier during HME processing. Most importantly, this work reports, for the very first time in the literature, the use of the F-H phase diagrams to predict the most appropriate HME processing window to drive higher cocrystal yield.

INTRODUCTION

Our previous work successfully demonstrated the feasibility of manufacturing (ibuprofen/isonicotinamide) Ibu-IsoNA cocrystals in the presence of a pharmaceutical excipient[1] using mechanochemical HME processing. From our previous work, it was shown that xylitol was the most appropriate (from the 4 selected). Xylitol is a chemically stable pharmaceutical excipient and food additive with a low melting viscosity at specified extrusion temperature[2]. In addition, xylitol was observed to exhibit rapid solidification upon cooling, which was also considered pertinent for the successful extrusion of a cocrystal suspended in the excipient matrix. The extruded cocrystal/xylitol suspensions exhibited further enhanced ibuprofen dissolution rate when compared with the analogous cocrystal extruded devoid of any excipient. However, the final cocrystal yield within the matrix was still unsatisfactory. In our previous study, a small amount of both reagents were rendered amorphous within the matrix during extrusion processing. Subsequently, increased cocrystal yield was observed during storage, particularly when the formulation was placed in a humid environment[3].

It has been indicated in the literature that cocrystallisation by melting or mechanochemical processes may not be as efficient as solution methods, due to limited activity of the reactant molecules[4]. But with the presence of a non-complementary carrier, both cocrystal reagents could 'dissolve' in the liquefied carrier, resulting in a similar cocrystallisation mechanism to traditional solvent approach, albeit in an increased viscosity environment (due to the viscous nature of the molten excipient). However, since the 'solvent' (matrix carrier) in a HME system will not be removed post processing, the solubility of the cocrystal within the carrier pool should be limited such that precipitation of the product is encouraged. It is therefore obvious that the phase behaviour between individual cocrystal components (including both the reagents and the product of cocrystallisation) and the matrix carrier may significantly influence the extent of cocrystal conversion. A carrier melt pool 'solvent' in which the reagents and the cocrystal show such distinctive solubility differences, or a temperature that drives a solubility difference

between reagents and cocrystal within a given carrier could be used to enhance the cocrystal yield. Therefore, this work is aimed at assessing the solubility of the cocrystal components in a given matrix as well as investigating how HME processing temperature settings may influence solubility and correlation to cocrystal yield. Two different methods have been used to achieve such aims, namely solubility parameter comparison and the adaptation of Flory-Huggins theory using the melting point depression method.

It has also been reported in the literature that increased mixing and shear intensity could facilitate cocrystal yield[5]. Therefore, not only can we expect temperature and miscibility to change yield but process parameters such as screw design that is known to alter extrudate properties[6], and operating efficiency[7] must be considered. Hence, another important aspect to this research paper is to identify the impact of screw geometry and to rationalize screw configuration for improved cocrystal yield during ternary extrusion processing. Screw configuration designs conveying increased shear intensity were investigated for their influence on cocrystal yield.

MATERIALS AND METHODOLOGY

Materials

Ibuprofen, isonicotinamide, and xylitol were purchased from Sigma-Aldrich (St. Louis, MO, USA). All other chemical reagents used were of analytical grade.

Calculating solubility parameters

The use of solubility parameters to predict the miscibility and/or compatibility of pharmaceutical materials has been extensively reported. Such information is often used to set criteria for excipient selection in formulation design[8–10], or for coformer selection in cocrystal screening[11,12]. Estimation of miscibility between any two components (Ibu vs. IsoNA, Ibu vs. xylitol, IsoNA vs. xylitol and, the 1:1 Ibu-IsoNA cocrystal vs. xylitol) within the cocrystal suspension system was performed by comparing the total solubility parameter (δ_t) for each individual component. δ_t was calculated using the Hansen partial solubility parameters (δ_d, δ_p & δ_h) based on the group contribution method of Fedors[13] and Van Krevelen-Hoftyzer[14,15]:

$$\delta_d = \frac{\sum F_{di}}{V}, \qquad \delta_p = \frac{\sqrt{\sum F_{pi}^2}}{V}, \qquad \delta_h = \sqrt{\frac{\sum E_i}{V}} \qquad \text{Equation 1}$$

$$\delta^2 = \delta_D^2 + \delta_P^2 + \delta_H^2 \qquad \text{Equation 2}$$

Where F_{di} is the group dispersion component contributing to the disperse forces δ_d, F_{pi} the plane symmetry factor giving polar group forces δ_p, E_i the group contribution to hydrogen bonding energy and V the molar volume from Hildebrand analysis.

Sample preparation for melting point depression measurements

All substances were desiccated over silica gel to guarantee minimum moisture content prior to use. The reference cocrystal was grown via slow evaporation from a methanol solution. The conversion from Ibu and IsoNA to their equimolar cocrystal was confirmed by thermal analysis, powder x-ray diffraction and spectroscopy as described in our previous work[1]. Binary physical mixtures containing compound A

(the reference cocrystal or individual parent reagent, respectively), and compound B (the matrix carrier xylitol) were prepared, using a mortar and pestle, at predetermined compositions (100%, 95%, 90%, 85%, 80%, 75% and 70% w/w of compound A) in triplicate. The resulting mixed powders were desiccated until further use.

Differential Scanning Calorimetry (DSC)

Melting point depression experiments for the binary physical mixtures were performed on a model DSC 8000 power compensation differential scanning calorimeter (Perkin-Elmer, Windsor, Berkshire, UK). The machine was calibrated, at the respective heating rates, for melting point and heat of fusion using indium and zinc, respectively, prior to the experiments. Both the reference and sample chambers were purged with dry nitrogen at a flow rate of 40mL/min to maintain an inert atmosphere. 3-5mg of sample was accurately weighed to aluminium pans and crimped using an aluminium pan lid. The crimped pan set was then subjected to a thermal ramp at 1°C/min from 80°C to 135°C. For samples containing IsoNA, a 200°C/min heating rate and 40mL/min purged helium were used to avoid compositional variations associated with IsoNA degradation at low heating rates (heating rate dependent weight loss observed in TGA analysis, data submitted in the supplementary material). Samples containing IsoNA were subjected to a 30-minute isothermal treatment at 100°C prior to the DSC ramping over a range from -60°C to 230°C. Such a pre-treatment was employed to provide an extended period so that any inadequate solubilisation caused by the fast heating[16] might be compensated. 100°C was chosen as the isothermal temperature as it was above the melting of xylitol, yet below the onset of significant IsoNA weight loss (120°C if heated at 1°C/min, data shown in supplementary material). The determination of the isothermal time, on the other hand, was based on whether stabilised depression of $\Delta H_{(IsoNA)}$ was attainable during preliminary screening (data included in supplementary document). All values of melting points used in this study were the end temperature of the melting event.

Powder X-ray Diffraction (PXRD)

PXRD was performed using a MiniFlex II desktop powder X-ray diffractometer (Rigaku Corporation, Kent, England). The machine is equipped with Cu Kα radiation, at a voltage of 30 kV and a current of 15 mA. The scanning was conducted across a 2Θ scanning range from 1.5-40° at 2.0°/min and a sample width of 0.03°. The peak area underneath the cocrystal characteristic peak at 3.3° 2Θ for each sample was used to determine the cocrystal yield[17]. A series of physical mixtures containing the reference cocrystal and xylitol at 10 different cocrystal loadings, 10, 20, 30, 40, 50, 60, 70, 80, 90 & 100% w/w, respectively, were prepared through gentle grinding. The blended samples were placed into a top-fill glass sample holder (0.2mm well depth) for analysis. The peak area was calculated using Integral Int. Calculation software (Integral analysis for windows, Version 6.0, Rigaku Corporation) with manual background subtraction and an integration region set between [2.400~4.050° 2θ]. A calibration curve, (R^2=0.998) was constructed using linear regression between the average peak area and cocrystal concentration in the blends. The calibration curve was validated for linearity, accuracy, precision, LoD and LoQ according to the methods recommended in the ICH guidelines[18]. The results from the construction and validation of the quantitative PXRD analysis were published as supplementary data for our previous work[1].

Determination of cocrystal yield

With the standard calibration curve established and validated, the cocrystal yield in the melt-extruded suspensions can be calculated as follows:

$$\text{Cocrystal yield (\%)} = \frac{\text{Measured cocrystal concentration (\%)}}{\text{Theoretical fully converted content (\%)}} \times 100\%$$

Where the theoretical fully converted content in this work was 50% as xylitol loading was kept constant at 50wt% for all cases.

Hot-melt extrusion (HME)

Hot-melt extrusion was conducted using a co-rotating 20:1 twin screw Rondol Microlab 10mm compounder (Rondol Technology Ltd., Staffordshire, UK) equipped with a force feeder and an open end. Raw materials were accurately weighed, pestle-mixed in a ceramic mortar, and subsequently fed at a fixed rate of 20rpm using the auxiliary single-screw force feeder. A screw speed of 10rpm was used for the main extruder in all extrusion experiments. Table 1 illustrates the temperature profile (TP) settings used in this work. In particular, the temperature for the feeding zone (Zone 0) for all formulations was kept constant at 60°C to allow adequate solid conveying from the feed hopper. The following Zone 1 was designed as the melting zone with temperature set at 80°C, 92°C, 100°C, 110°C and 115°C, respectively. To ensure the production of a solid extrudate rather than a melt pool at the barrel exit, Zone 2 & Zone 3 were designed as cooling zones and set with gradually decreasing temperatures (Table 1).

As detailed in Table 2, three different screw configuration profiles (SCP) were applied to modify the mixing and shear intensities and to understand the link to cocrystal yield during HME. SCP1 was assembled using conveying elements only. SCP2 incorporated two kneading regions each configured as a 90° neutral-staggered kneading block sandwiched by two 60° forward-staggered kneading blocks. In SCP3, additional kneading blocks were included in each kneading region to provide further enhanced shearing within the melt stream.

Extrusion was repeated in triplcate for each formulation and the average residence time and system torque were recorded in Table 3. The resulting extrudates were collected directly from the open barrel end and subsequently pulverized using a mortar and pestle once cooled. The powdered samples were sieved through a 212μm mesh sieve (Scientific Laboratory Supplies Ltd, Nottingham) and then desiccated in non-humid environment prior to further analysis. Note that all formulations extruded in this work contained a fixed xylitol content of 50% w/w.

Statistical analysis

Statistical analyses were conducted using GraphPad Prism one-way analysis of variance with Tukey's multiple comparison tests. The confidence interval was set automatically as 95%. The computed statistics provide a significance value (P) for each individual comparison. A "P" value less than than 0.05 indicates significant difference.

FLORY-HUGGINS THEORY AND DATA TREATMENT

Flory-Huggins theory is a comprehensively used mathematical theory, developed independently by Flory[19,20] and Huggins[21,22], for modelling the thermodynamics of binary polymer-solvent mixtures. In this model, the size disparity between the two components is taken into account when determining the entropy of mixing of a binary system consisting of unequal-sized molecules. The theory assumes hypothetical lattice sites that accommodates either an individual solvent molecule or a polymer chain segment. It is assumed that the macromolecular polymer is equivalently divided into a number of chain segments that each occupies the same volume on a lattice as a solvent molecule in order to utilise the usual expression of entropy of mixing. The free energy of mixing ΔG_{mix} for such a binary system, according to F-H theory, can be expressed using Eq. 3[23]:

$$\frac{\Delta G_{mix}}{RT} = \Phi \ln \Phi + \frac{(1-\Phi)}{m} \ln(1-\Phi) + \chi\Phi(1-\Phi)$$

Equation 3

Where Φ is the volume fraction of solvent (the small molecular component), R is the molar gas constant, T is the temperature in the Kelvin, m is the number of polymer chain segments (typically calculated as the ratio of the volume of a polymer chain to that of a solvent molecule), and χ is the F-H interaction parameter between polymer and solvent molecules[19]. In such an expression, the obtained ΔG_{mix} shows clear composition dependency. Mathematically, the entropy factor (the first two terms on the right-hand side of Eq. 3) of the expression favours mixing by resulting in non-positive numerical values at all times. The enthalpy factor (the third term), in contrast, shows influence on the mixing preference through the value of χ. For systems exhibiting adhesive bonds favouring miscibility (negative χ values) and/or no specific bonding between species whatsoever (χ = 0), the ΔG_{mix} can remain negative throughout the entire composition range. Whereas for systems that exhibit unfavourable mixing (positive χ values), the ΔG_{mix} only remains negative until a certain threshold value of χ and becomes positive at points beyond.

By adapting the concept of the F-H theory, melting point depression theory [24,25] may be used in the calculation of χ value for drug-polymer binaries where the following equations, Eq. 4 and Eq. 5, are applied[16,26–31]:

$$\frac{1}{T_m} - \frac{1}{T_m^0} = -\frac{R}{\Delta H}\left[\ln \Phi + \left(1 - \frac{1}{m}\right)(1 - \Phi) + \chi(1 - \Phi)^2\right]$$

Equation 4

$$\chi = \frac{\frac{1}{T_m} - \frac{1}{T_m^0}}{-\frac{R}{\Delta H}(1 - \Phi)^2} - \frac{\ln \Phi}{(1 - \Phi)^2} - \frac{1 - \frac{1}{m}}{1 - \Phi}$$

Equation 5

Where T_m is the melting temperature of drug in the binary mixture; T_m^0 and ΔH are the melting temperature and the enthalpy of fusion, respectively, for the pure drug substance.

Based on the expression in Eq. 5, the estimation of the dimensionless, enthalpic energy parameter χ is related to both temperature and composition. Using experimentally obtained T_m values for binary mixtures of different drug-polymer compositions, the corresponding value of χ can be calculated. In practice, however, the measurement of T_m is always rendered unfeasible at low drug loadings. Ability to extrapolate the value of χ beyond experimentally feasible temperatures is then crucial to the establishment of phase behaviour throughout the entire composition range. In the current literature, a first order relationship between χ and the reciprocal temperature (Eq. 6) has been commonly used for such purposes[23,29]:

$$\chi = A + \frac{B}{T}$$

Equation 6

Constants A and B can be fitted using the experimental data, allowing the free energy of mixing expression to be become:

$$\frac{\Delta G_{mix}}{RT} = \Phi \ln \Phi + \frac{1 - \Phi}{m}\ln(1 - \Phi) + \Phi(1 - \Phi)\left(A + \frac{B}{T}\right)$$

Equation 7

Additionally, by setting the second derivative of the ΔG_{mix} to Zero, one can achieve Eq. 8 to determine the position of the spinodal curve[32], which depicts the boundary of phase separation in the solid state:

$$T_s = \frac{2B}{\frac{1}{\phi} + \frac{1}{m(1-\phi)} - 2A}$$

Equation 8

RESULTS AND DISCUSSION

Cocrystallisation using a conventional solution approach is generally conducted in ternary systems consisting of a conformer, drug and a solvent or a mixture of solvents. Solubility information between individual cocrystal components and the solvent is fundamental in establishing phase diagrams that are generally used to describe the conditions needed for cocrystal formation[33–37]. Moreover, it has been shown that coformer solubility in solvent during liquid-asssited mechanochemical synthesis plays an important role, influencing cocrystallisation efficiency[4,38–43].

In our work, we consider the synthesis of a cocrystal in a molten carrier to be similar to that in the presence of a traditional organic solvent. The liquefied carrier serves as a viscous solvent to accommodate the parent reagents, hence providing increased degrees of freedom for hetero-molecular collision and thus improved cocrystallisation efficiency. In previous research, it has been suggested that the solvent should not be capable of forming secondary interactions with any cocrystal reagents such that the interactions between the reagents are still favoured. In respect of HME, processing conditions may be controlled in order to enhance interaction between cocrystal reagents and limit reaction with meltable carrier 'solvent'[44,45]. In addition, we should also remember that unlike a traditional organic solvent used for either solvent-based cocrystallisation or liquid-assisted grinding, the molten carrier used during HME will not evaporate after processing, but rather remains as a matrix. As such the pharmaceutical excipient used as a matrix carrier should be suitable to meet the end use of the drug product. In particular, the dispersed cocrystal phase must have limited solubility in the matrix carrier at decreased temperature when the formulation exits the extruder in the solid-state. Without this condition being met there may be a high probability that an amorphous dispersion of individual coformer molecules, rather than a cocrystal suspension would form within the carrier[46].

To aid understanding of this hypothesis, an illustration showing the preparation of cocrystal suspensions in a single-step HME is provided in Figure 1. Using this method, the manufacture of cocrystal suspensions may be regarded as a sequence of

events in the direction of melt flow. Ideally, the ternary physical mixture is fed into the extruder feed zone as mixed solids. The mixed solids are then conveyed to a melting zone where a melt pool forms. The presence of such a melt pool provides a medium for cocrystallisation and additionally may also significantly improve reaction kinetics due to the increased mobility within the molten matrix[47]. The processing temperature in the following zone should be decreased sufficiently to assist precipitation of the newly formed cocrystals from the carrier melt, whilst the final zone ought to be designed with a further decreased temperature to ensure solidification of the carrier, and thus, formation of an intimately mixed cocrystal suspension. Consequently, it is extremely important to understand solubility behaviour and miscibility of individual cocrystal components and the carrier. Interestingly, in the scenario presented, solubility and component miscibility must be considered both in the melt and also in the solid-state. In this work, we present two extensively reported methods for the purposes of advancing our understanding of this complex cocrystal manufacturing process.

Solubility Parameters

The Hansen solubility parameters (HSP) calculated using the group contribution method has enabled the prediction of solid-solid solubility of pharmaceutical relevant materials[8,9]. For drug-excipient combinations, the Forster predictions consider a $\Delta\delta_t < 7.0$ MPa$^{1/2}$ indicative of significant miscibility and formation of glass solutions during melt-extrusion, whereas a $\Delta\delta_t > 10.0$ MPa$^{1/2}$ denotes a lack of miscibility and limited ability to form glass solutions[10]. Later, Velaga *et al.*, explored the correlation between solubility parameter calculations, predicted drug-coformer miscibility and the feasibility of cocrystallisation[11]. In this important work, it was shown that those systems capable of successfully forming cocrystals were manufactured from systems that were miscible. The authors therefore concluded that drug-coformer miscibility was necessary in order to attain cocrystallisation, and that the use of solubility parameters was an efficient method for screening coformer candidates.

In the light of the above, our current study considered that Ibu and IsoNA should show significant good miscibility thus encouraging cocrystallisation. Moreover, our selected carrier (Xylitol) should exhibit limited miscibility with the formed cocrystal. Within this investigation our hypothesis is that dissolution of the parent reagents within molten xylitol could increase activity of the reactants hence increasing interspecies collision, leading to improved cocrystal yield. However, interaction between xylitol and each individual cocrystal reagent must not surpass that between the parent reagents.

The solubility parameter values for parent reagents, cocrysal and xylitol were calculated and compared. Table 4 gives a list of the identified component group contributions and the calculated total solubility parameter for each compound. The subsequent calculation of the total solubility parameter difference $\Delta\delta_t$, is as follows: $\Delta\delta_t$ (Ibu/IsoNA) is 1.95 $MPa^{1/2}$, $\Delta\delta_t$ (Ibu/xylitol) and $\Delta\delta_t$ (IsoNA/xylitol) are 13.56 $MPa^{1/2}$ and 11.61 $MPa^{1/2}$, respectively, whilst $\Delta\delta_t$ (cocrystal & xylitol) is 13.74 $MPa^{1/2}$. According to Forster *et al.*, the $\Delta\delta_t$ values obtained confirm, theoretically, that Ibu and IsoNA are strongly miscible, whilst xylitol is less miscible with both the cocrystal reagents and the respective equimolar cocrystal. The predicted immiscibility between xylitol and the Ibu-IsoNA cocrystal may be beneficial in precipitation of cocrystal product from the excipient following extrusion. Unlike cocrystallisation using conventional solvents in which cocrystal production is facilitated through evaporation of solvent, formulating a cocrystal suspension via HME is fundamentally different in the sense that the excipient carrier solidifies rather than evaporates after processing. Therefore precipitation, in such cases, can only occur when the newly formed cocrystal exhibits a significantly reduced miscibility/solubility with the carrier excipient. Interestingly, the limited miscibility predicted using the solubility parameter approach between xylitol and each individual parent reagent (Ibu and IsoNA), presents a complex scenario for evaluation of such a system. In such cases the limited miscibility may render the presence of xylitol a physical hindrance thus preventing reaction of the parent reagents and formation of cocrystal. However, it must be noted that the calculated solubility parameter values do not take in to account the shearing forces and

temperatures involved during extrusion, which may promote reaction of the two components. Moreover, miscibility predictions are very much dependent upon temperature and the relationship to the solubility parameter. Comprehensive group contribution information throughout a greater temperature scale other than 25°C[48,49] is still lacking, rendering the HSP method somewhat less useful while assessing the mixing behaviour at significantly elevated temperatures during the HME processing. Furthermore, in our previous work describing the manufacture of cocrystals via HME we indeed demonstrated the successful formation of an equimolar Ibu-IsoNA cocrystal from a ternary mixture with xylitol[1].

Melting Point Depression Measurement and Construction of Phase Diagrams

The use of Flory-Huggins theory in combination with melting point depression measurements, has recently been utilised to better understand the relationship between binary mixing behaviour and temperature. In particular, F-H theory has been shown to be useful in determining the impact of processing temperature on the miscibility of components during melt extrusion[16,29,31,50]. Although F-H theory has been used for polymeric and other viscous systems, the high melt or rubber viscosity provide a kinetic barrier to dissolution. The hindered mobility in these systems often leads to an underestimation of solubility. In this current study involving xylitol, a small molecular weight sugar alcohol, the similarity of molecular weight between components and the low viscosity of xylitol reduce the likelihood of underestimation. In the original F-H theory, a hypothetical 'lattice' in space is assumed as the spatial volume that a polymer chain segment or a solvent molecule occupies. The fact that both the solute and solvent in this case are small molecules reduces the extent of dissimilarity in molecular size. In our consideration, instead of assuming a hypothetical space, we took into account the size dissimilarity directly by calculating the volume ratio of a carrier molecule to a drug molecule using their true densities and respective molecular weights (Table 5).

Ibuprofen, has a lower melting temperature (76.86±0.08°C) relative to xylitol (95.32±0.14°C) and thus it is reasonable to assess xylitol solubility in molten

ibuprofen. It is also worth noting that when determining the mixing between xylitol and ibuprofen, xylitol is considered the 'solute' while ibuprofen is considered the 'solvent'. In the design of the latter melt extrusion experiments, ibuprofen and xylitol were subjected to fusion simultaneously. The true density, T_m and ΔH for IBU, IsoNA, xylitol and the reference cocrystal are listed in Table 5. The melting endotherms are shown in Figure 2 for ibuprofen-xylitol, isonicotinamide-xylitol and cocrystal-xylitol binary systems, respectively. It is worth noting that a DSC heating rate of 1°C/min was applied to both the xylitol/Ibu and cocrystal/xylitol systems, whilst 200°C/min was employed for the IsoNA/xylitol system. This was because IsoNA was discovered to sublime hence undergoing tremendous weight loss before reaching its melting point. Such sublimation was heating rate-dependent, with prominently increased loss of weight if sample was treated with extremely slow heating such as 1°C/min, but negligible weight loss if heated using 200°C/min (See Appendix 1 in the supplementary document). Our previous publication has investigated the influence of DSC heating rate upon the construction of drug-polymer miscibility phase diagram when applying the FH theory to the melting point depression data[16]. It was shown in that work the use of high DSC heating rates could result in underestimation of the metastable region and inaccurate prediction of a poor miscibility limit. The authors attributed such inaccuracy to inadequate dissolution of molecules from within the drug crystalline lattice into the polymer, when increased DSC heating rates were applied. However, in the current work, the dissolution of IsoNA in molten xylitol does not necessarily suffer from the same extent of time-dependence, since xylitol is a small molecular component with significantly lower melting viscosity. Though that being said, a compensational isotherm was conferred on the IsoNA/xylitol mixtures, prior to the DSC experiments. This isotherm was performed at 100°C, well below the onset of IsoNA weight loss (Appendix 1 in the supplementary document), but above the melting of xylitol, sufficient to create a melt pool of xylitol for IsoNA to dissolve in. A time frame of 30 min was selected from a series of tested periods (15, 30 and 45 min) since it provided a stabilised heat of fusion depression (see Appendix 2 in the supplementary document).

Melting depression was evident in each system, for example in the xylitol/Ibu blends, the end point for the xylitol melting was measured to shift gradually from 95.32±0.14°C to 94.84±0.07°C with gradual increase of the ibuprofen content from 0-30wt% (Figure 2a, for mean and standard deviation of individual measurement please see Appendix 3 in the supplementary document). Interestingly, although ibuprofen melted at a lower temperature than xylitol, the presence of the latter was observed to depress the melting of ibuprofen from 78.86±0.08°C to (76.44±0.10°C). Similarly, increase of the xylitol content in both IsoNA/xylitol and cocrystal/xylitol systems also resulted depression of IsoNA and the cocrystal melting from 169.79±1.62°C to 150.52±0.42°C (Figure 2b), and from 120.96±0.06°C to 115.43±0.07°C (Figure 2c), respectively (see Appendices 4 and 5 in the supplementary document for mean and standard deviation of individual measurement). A small endothermic event (141.29±0.21 °C) was also observed on the pure IsoNA DSC thermogram, shortly prior to the main melting at 169.79±1.62°C (Figure 2b). This corresponds to the thermal behaviour of IsoNA polymorph 2 (CSD refcodes EHOWIH, EHOWIH01)[51]. The small initial endotherm has been previously reported to be the result of solid-solid phase transition into modified forms which would then melt as IsoNA polymorph 2[52].

Using the melting depression data, the Flory-Huggins interaction parameter, χ, was calculated for each respect system (across experimentally measurable temperatures) using Eq. 5 and plotted against the corresponding reciprocal of T_m in Figure 3. Linear regression shows reasonably good fits ($R>0.94$) for all three systems. As discussed before, although our previous paper has shown the impact of heating rate on the construction of the F-H phase diagrams, and more directly on the values of χ[16], such impact was again considered not significant in the current work, due to the limited kinetic hindrance (since all species involved were small molecules) present in the system. Indeed, in Figure 3b, negative χ values were calculated for the IsoNA/xylitol blends with increased negativity when increasing the xylitol content. A negative A value calculated from the linear fit (Eq. 6), in particular, suggests negative Gibb's free energy and favourable mixing between the

two species due to favourable entropic contributions in the system. Interestingly for the xylitol/ibuprofen and the cocrystal/xylitol blends, both χ-1/T plots resulted in positive A values instead (Figure 3a and 3c, respectively), suggesting unfavourable mixing and positive Gibb's free energy at the depressed melting temperatures of xylitol and the cocrystal.

A plot of $\Delta G_{mix}/RT$ versus compound fraction for each system is shown in Figure 4 based on Eq. 7, denoting the variation of free energy of mixing as a function of both composition and temperature. It is worth nothing that the temperatures chosen for the calculation of $\Delta G_{mix}/RT$ were the nearest integers to the following criteria: (1) above ibuprofen melting endpoint – 80°C; (2) onset of xylitol melting – 92°C; (3) end of xylitol melting – 95°C; (4) onset of the equimolar Ibu-IsoNA cocrystal – 120°C; and (5) intermediate temperatures between (3) and (4) – 100°C, 110°C and 115°C, respectively. Generally speaking, a negative energy value is indicative of mixing in which attraction forces between species are stronger than that between like molecules promoting the occurrence of a homogeneous phase, whereas a positive energy value signifies immiscibility. The shape of the energy curve at a specific temperature is also informative. A concave curve is often observed in homogeneous phases revealing negative energy values throughout the entire composition range. A convex shape, on the other hand, suggests spontaneous phase separation for all compositions at this temperature. A sigmoidal curve, therefore, is indicative of concentration dependent phase behaviour at the defined temperature.

In Figure 4a, it is shown that the energy of mixing between ibuprofen and xylitol is almost zero throughout the entire composition range when the temperature is 95°C. Concave energy curves are observed for both 92°C and 80°C, while convex curves are observed from 100°C to 120°C. Such energy diagrams suggest that ibuprofen is less miscible with xylitol when temperature elevates, agreeing with the previously obtained positive A and χ values. A similar trend is also observed for the cocrystal/xylitol blends in Figure 4c where the energy curve changes from a concave profile at 80°C (favourable mixing) to approximating a plateau (majority of the energy values just above zero) when the temperature reaches 115°C. Further

increase of the temperature to 120°C resulted in a convex energy curve, suggesting limited miscibility at such a temperature. The IsoNA/xylitol blends, on the other hand, exhibited concave energy curves from 110-120°C (Figure 4b), indicative of complete miscibility between IsoNA and xylitol across the entire composition range at these temperatures. Interestingly, although the energy curve was sigmoidal at 100°C, all the values of $\Delta G_{mix}/RT$ were negative, suggesting favoured interspecies mixing at this temperature too.

Derived from these energy curves, the thermodynamic (temperature-composition) binary phase diagrams were constructed for xylitol/ibuprofen, IsoNA/xylitol and the reference cocrystal/xylitol mixtures, respectively, enabling the prediction of binary miscibility as a function of temperature. From Figures 5a and 5c, it can be seen that a Lower Critical Solution Temperature (LCST) behaviour was evident for both the xylitol/ibuprofen and the cocrystal/xylitol systems, with the calculated critical temperatures to be approximately 95°C and 114°C, respectively. The LCST is the shared minimum of the two F-H theoretical curves, the concave spinodal and binodal lines, respectively. A LCST behaviour denotes complete miscibility in all proportions at temperatures below the LCST. In the previous energy curves, a plateau line was reached at 95°C to distinguish the boundary between complete miscibility (concave energy curve) and limited miscibility between xylitol and ibuprofen. A similar plateau was also observed at 115°C to denote complete and limited miscibility boundary between the cocrystal and xylitol. Therefore, the LCST behaviour observed for the two systems agrees with the previous energy curve indications and is suggesting complete miscibility between xylitol and ibuprofen below 95°C and that between the cocrystal and xylitol below 114°C (or 115°C if not taking into account the 1°C discrepancy between the LCST and the $\Delta G_{mix}/RT$ plateau), respectively. Such result is most interesting yet counter-intuitive as it is advising complete miscibility between these species at room temperature. Although the existence of an LCST for small molecules is rare, there are previous reports of immiscibility between ibuprofen and xylitol when both compounds are molten[9]. Complete miscibility between the Ibu-IsoNA cocrystal and xylitol, on the other hand, could contradict with the "immiscible with newly formed

cocrystal" criteria for carrier screening in the first place. However, one must remember that all species are in the solid crystalline state at room temperature, hence the likelihood of cocrystal dissolution in the rigid xylitol crystalline lattices would be extremely small due to strong kinetic hindrance.

From Figure 5b, an Upper Critical Solution Temperature (UCST) behaviour is observed for the IsoNA/xylitol system with the critical temperature calculated to be 110°C. Such result indicates complete IsoNA-xylitol miscibility at temperatures greater than 110°C, in conformity with the miscibility boundary suggested by the concave $\Delta G_{mix}/RT$ curves in Figure 4b. However, it is worth noting that the negative $\Delta G_{mix}/RT$ values at all proportions on the sigmoidal energy curve at 100°C (Figure 4b), although signifies thermodynamically favoured mixing, still exhibits a 10°C difference than what would be required for ideal mixing (UCST).

Hot-melt Extrusion with Predetermined Temperature Profiles and Screw Configuration Profiles

Phase Diagrams and relevance to Processing

From melting depression data previously discussed, ideal mixing would occur below 95°C between ibuprofen and xylitol, however above 110°C to ensure (or at least higher than 100°C to favour) dissolution of isonicotinamide in the molten xylitol. Moreover, processing should be carried out above 115°C to facilitate precipitation of cocrystal product from the xylitol melt (LCST at 114°C and all-proportion negative $\Delta G_{mix}/RT$ values above 115°C). Using this theoretical framework makes it impossible to identify a processing window that would be ideal for mixing of parent reagents with xylitol whilst encouraging precipitation of the cocrystal product (Figure 6). Despite this, our previous work successfully prepared an equimolar Ibu-IsoNA cocrystal (albeit with relatively low yield) at 92°C, the temperature being selected to correspond to the onset melting temperature for xylitol, in a HAAKE Minilab conical twin-screw extruder[1].

In order to understand how useful the F-H theory is with respect to manufacture of cocrystal material and in identifying relevant processing windows, temperatures

previously shown to be critical in both the energy curves and T-Φ phase diagrams (80, 95, 100, 110 and 115°C, respectively) were used for Zone 1 during extrusion. This zone was used as a melt zone for the ternary system, consisting of an equimolar Ibu-IsoNA premix blended with xylitol at a 1:1 mass ratio. The feed zone (Zone 0) upstream to Zone 1 was kept constant at 60°C to allow adequate solid conveying. Zones 2 and 3 downstream to the melt Zone 1 were set at gradually cooled temperatures to ensure solidification of the extrudates. The respective temperature profiles (TPs) were named as TP1-TP5 (Table 1), respectively.

Extrusion trials 1-5 were conducted with a full set of conveying screw elements (SCP1). As shown in Figure 7, when SCP1 was used, temperature profiles TP1, TP2 and TP3 resulted in low but gradually increasing cocrystal yields (9.0±0.2%, 9.7±1.2% and, 12.6±2.0% respectively). TP4 gave the highest yield of 31.4±1.9% with TP5 showing a small but significant decrease in yield to 22.1±1.2%. Interestingly, according to previous phase diagram predictions, although 110°C (TP4 melting zone temperature) is favouring IsoNA dissolution in the xylitol melt, this temperature is unfavourable for miscibility between xylitol and ibuprofen. If based on the original hypothesis that dissolution of both parent coformers is required for cocrystallisation, TP4 should result in just as low cocrystal yield as TP1 and TP2. However, it was clearly evident that IsoNA/xylitol miscibility (as with TP4) played a more dominant role in driving cocrystallisation to higher yield, whereas the influence of xylitol/ibuprofen miscibility (as with TPs1-3) was much less pronounced. This is probably because when dissolved in the xylitol melt, the conformational freedom open to IsoNA molecules is significantly enhanced at various interfaces, so there is greater probability for molecular collision[53]. With regard to ibuprofen, on the other hand, melting of the drug occurred at all investigated processing temperatures, and thus, there was already a high ibuprofen molecular mobility[5]. It also appeared that there was no significant impact on cocrystal yield whether molten ibuprofen was miscible (TP1) or immiscible (TP2 & TP3) with xylitol. In fact, FTIR analysis within our preliminary investigations showed no evidence of molecular interaction between ibuprofen and xylitol molecules in a mixture prepared by melting followed with quench cooling. This

would have created almost a competing environment between the molten ibuprofen and the molten xylitol to interact with the dissolved IsoNA molecules. Therefore, it would be crucial that the interactions responsible for IsoNA-xylitol miscibility are not substantially stronger than that responsible for the ibuprofen-IsoNA cocrystallisation.

It is also worth noting that when using 100°C as the melting zone temperature (TP3), although the energy curve predicted negative ΔG_{mix} at all compositions (suggesting favoured IsoNA/xylitol mixing), the cocrystal conversion yielded from TP3 (12.6±2.0%) was only 1/3 of that from TP4 (31.4±1.9%). Since the temperature setting (110°C) used in TP4 was the UCST in the binary system denoting boundary of complete IsoNA/xylitol miscibility, significant cocrystal yield increasing from TP4 is suggesting that the critical temperature prediction using the T-ϕ phase diagram may offer more guidance in selecting processing temperature rather than a simple reliance on temperatures when ΔG_{mix} is negative.

The phase diagrams also suggested cocrystal/xylitol phase separation at temperatures higher than 114°C (the LCST). Since Zone 2 and Zone 3 were set at gradually decreasing temperatures to allow sufficient solidification for xylitol, it is presumed that the Ibu-IsoNA cocrystal would precipitate out from the xylitol melt in the melting Zone 1, where phase separation is thermodynamically favoured. Moreover, the precipitation of the cocrystal from xylitol might drive further dissolution of IsoNA into the molten carrier. Therefore, it was anticipated that TP5, having 115°C set as the melting zone temperature, should result in further increased cocrystal yield than TP4. However, with full conveying screw geometry (SCP1), the resulted yield from TP5 was only 2/3 (22.1±1.2%) of that from TP4. Although such result seems to suggest inaccuracy of the cocrystal/xylitol phase diagram predictions, one should remember that, in extrusion, it is common to have a higher melt temperature than the set values. Such temperature variations are typically the result of local temperature fluctuations derived from the frictional heat generated during shearing. In the current work, the LCST denoting cocrystal/xylitol phase separation (114°C) was too close to the onset of cocrystal melting (120.21±0.26°C).

With increasing cocrystal yield and hence increased amount of solid content, the frictional heat accumulation increases, and so does the regional temperature. Once the local temperature rise approaches close to the cocrystal melting temperature, the newly formed cocrystal would start to melt. If the cocrystal melting overweighs their increased formation, a reduced overall yield (relative to TP4) would be measured. Therefore, while using the T-ϕ phase diagram to predict the HME processing window for cocrystal suspensions, the influence of the mechanical shearing upon phase transition, such as melting, of the cocrystal components should not be ignored.

Screw Configuration and Cocrystal Yield

When extruding the binary mixture of a coformer pair, increased mixing intensity has been reported to contribute to improved cocrystal yield[5]. It is of interest to see how varying the level of mixing could impact upon cocrystal yield, particularly in this complex ternary system consisting of a coformer pair and a matrix carrier (xylitol). More importantly, it is interesting to understand how this information can be used to design a screw configuration that drives improved cocrystallisation.

Consequently, the ternary blend consisting of premixed equimolar Ibu-IsoNA and xylitol at 50:50 weight ratio was subjected to two additional screw configurations SCP2 and SCP3, respectively. Initially, both the SCP2 and SCP3 contain forward conveying elements for the feed Zone 0 to ensure material transport (Figure 8a). To facilitate mixing and the subsequent formation of cocrystals, kneading blocks were introduced to Zone 1. The kneading block designs are the most commonly used mixing element among numerous element designs for co-rotating twin-screw extruders. This is due to their mixing efficiency and self-wiping nature. A block of kneading discs, are usually described as stagger angle between two adjacent discs, number of discs in one block and overall length of the block. The kneading blocks used in this study include 60/4/10 elements (60° stagger angle with 4 discs forming a 10mm long block), and 90/4/10 elements for SCP2 and SCP3, respectively.

Generally speaking, for kneading blocks that are arranged in a forward conveying direction, a smaller stagger angle provides more positive melt flow (pumping capability). A kneading element with a perpendicular disc design (a 90° stagger angle) is called a neutral kneading block that has neither forward nor reverse conveying attributes. The conveying of materials through a neutral block is entirely dependent upon forward conveying elements upstream the block to compensate for the lack of conveying action in the neutral kneading region[54,55]. Therefore, an increased number of neutral kneading blocks usually results in increased extrusion residence time owing to reduced forward conveying capacity. Figure 8b shows the detailed kneading block arrangement employed in SCP2. A 90/4/10 block was sandwiched between two 60/4/10 blocks. A gradually increasing then 'phase out' sequence is usually deemed necessary to provide a transition between complete forward flow and complete stagnation so that local pressure within the neutral kneading region does not increase dramatically. The same sequence was used both in Zone 1 and between Zone 2 and Zone 3 in (Table 2, SCP2). It is worth noting that two separate kneading regions were used to prevent excessive stagnation of the melt flow. The measured cocrystal yields are shown in Table 3, (SCP 2, formulations 6-10). In general, the percent cocrystal yield was dependent upon Zone 1 temperature setting, with 13.8±0.3%, 13.9±0.1%, 20.6±0.4% and 44.2±0.3% measured for TP1-4, respectively, and 30.5±0.8% for TP5. The incorporation of kneading sections was evidently in favour of increased cocrystal yield. Moreover, the overall correlation between the cocrystal yield and the TP settings was still in agreement with what had been previously achieved using full convey screw configuration (SCP1). TP5, although anticipated to offer further increased cocrystal yield according to the T-ϕ phase diagram predictions, resulted in a reduced yield than TP4. This, again, emphasises the importance of mechanical input during HME, its impact upon local temperature fluctuation and phase transition (i.e. melting) of the produced cocrystal.

In addition, the stagger angle between adjacent kneading discs controls the inter-disk leakage, which dictates whether the kneading unit is more prone to dispersive

or distributive mixing (Figure 9). Kneading elements that show a smaller stagger angle or broader kneading disc thickness typically contribute to increased dispersive mixing, whereas those with larger stagger angle or narrower disc thickness result in increased distributive mixing[7,55–58]. As suggested by the phase diagram and also identified in previous extrusion trials Zone 1 is the region of the extruder where there are melting of ibuprofen and xylitol, dissolution of IsoNA into molten xylitol, and precipitation of cocrystal from the xylitol melt. Given the complexity involved in this zone, an attempt was made to separate the nature of mixing in Zone 1. As Table 2 shows, two 0/2/10 sections were introduced to Zone 1 in SCP3 in order to provide additional dispersive mixing. These two half sections were configured as shown in Figure 8c. The incorporation of such elements to the first kneading region was to enhance dissolution of IsoNA in xylitol, a process that was shown to be essential for cocrystallisation. It was considered that the dispersive mixing sections might improve IsoNA-xylitol molecular dispersion as well as facilitate Ibu-IsoNA molecular collision, hence improving cocrystallisation efficiency[59–62]. Whilst in the second kneading region, the SCP3 employed an additional 90/4/10 block in order to offer prolonged distributive mixing, thus improving distribution of the cocrystal particulates suspended within the xylitol matrix without further reducing the particle size and rendering them amorphous. Further enhanced cocrystal yield was obtained with SCP3 at all extrusion TP settings. In particular, TPs 1-4 resulted in 19.9±3.1%, 18.1±0.9%, 35.0±2.9% and, 58.8±1.8% cocrystal yielding, respectively, whilst TP5 resulted in a 39.8±1.7% yield. All results show good agreement with our SCP design hypothesis and previous discussion.

CONCLUSION

In this study, we report for the first time the use of phase diagrams derived from F-H theory in (1) determining miscibility behaviour; (2) selection of matrix carrier and; (3) providing guidance on HME processing temperature for cocrystal ternary systems. The use of small-scale thermal analysis and the adaptation of the Flory-Huggins theory provide useful information such as binary solubility and correlation between such solubility and temperature. This information was used in an attempt to predict the conditions under which cocrystal yield could be significantly improved. The construction of phase diagrams was useful in determining the HME processing temperature at which cocrystal yield may be thermodynamically favoured whereas screw profile experiments have shown that screw geometry modification can also be employed to alter cocrystal yield. By optimum selection of processing temperature and careful choice of extruder screw design, we have obtained cocrystal yield of approximately 60% in the presence of a matrix carrier. It is important to note that such a conversion ratio was achieved on a bench-top lab-scale extrusion compounder. Through the use of larger processing equipment, greater flexibility would be available in terms of both temperature setting and screw profile across the barrel. This may allow for improved control and hence further increased yield of cocrystal during scale-up.

Table 1 Temperature profile settings TP1~TP5 designed to provide different thermodynamic environment for various degrees of mixing among raw ingredients.

	Zone 0 °C	Zone 1 °C	Zone 2 °C	Zone 3 °C
TP1	60	80	80	80
TP2	60	95	85	80
TP3	60	100	90	80
TP4	60	110	95	80
TP5	60	115	100	80
Extrusion direction				

Table 2 Specification of the screw configuration profile on one assembly shaft arranged from underneath the feed throat to the discharge end.

No.*	SCP1	No.	SCP2	No.	SCP3
	Element type		Element type		Element type
19	Forward conveying	6	Forward conveying	6	Forward conveying
1	End unit	1	60° kneading	0.75	60° kneading
		1	90° kneading	0.5	0° kneading
		1	60° kneading	0.5	60° kneading
	Screw tip	4	Forward conveying	0.5	0° kneading
		1	60° kneading	0.75	90° kneading
		1	90° kneading	1	60° kneading
		1	60° kneading	3	Forward conveying
		3	Forward conveying	1	60° kneading
		1	End unit	2	90° kneading
			Screw tip	1	60° kneading
				2	Forward conveying
				1	End unit
					Screw tip

* Number of element unit (Length/Diameter).

Table 3 Nomenclature and process conditions for the hot-melt extruded 1:1 Ibu-IsoNA cocrystal suspensions. Note that Ibu and IsoNA were premixed at a 1:1 molar ratio, whereas the weight fraction of xylitol in the ternary mixture was 50wt% for all extruded formulations.

Formulation	Temperature profile	Screw configuration profile	Zone 0	Zone 1	Zone 2	Zone 3	Cocrystal Yield (%)
			Actual recordings (°C)				
1	TP1	SCP1	60.3±0.28	80.2±0.14	80.0±0.07	80.0±0.00	9.0 ± 0.2
2	TP2		60.4±0.64	95.2±0.35	87.8±1.20	80.2±0.07	9.7 ± 1.2
3	TP3		63.0±1.20	100.2±0.28	91.6±0.49	82.6±0.57	12.6 ± 2.0
4	TP4		66.6±2.33	110.2±0.21	101.4±0.28	87.9±0.57	31.4 ± 1.9
5	TP5		66.4±2.05	115.4±0.14	104.1±0.28	89.2±0.71	22.1 ± 1.2
6	TP1	SCP2	60.1±0.14	80.2±0.07	80.65±0.21	80.0±0.07	13.8 ± 0.3
7	TP2		60.2±0.21	95.1±0.14	88.2±0.21	80.3±0.14	13.9 ± 0.1
8	TP3		61.6±0.49	100.2±0.14	93.2±0.28	88.3±0.28	20.6 ± 0.4
9	TP4		63.0±0.57	110.2±0.07	105.3±0.57	90.2±3.04	44.2 ± 0.3
10	TP5		65.9±0.14	115.4±0.28	107.0±0.14	91.5±0.85	30.5 ± 0.8
11	TP1	SCP3	60.0±0.07	80.4±0.42	81.1±0.28	80.0±0.07	19.9 ± 3.1
12	TP2		60.0±0.00	95.0±0.00	87.8±0.99	81.1±1.56	18.1 ± 0.9
13	TP3		60.3±0.28	100.2±0.28	95.0±0.35	86.0±2.69	35.0 ± 2.9
14	TP4		62.8±0.35	110.0±0.07	102.6±2.62	89.0±4.17	58.8 ± 1.8
15	TP5		65.5±0.42	115.1±0.14	107.0±0.21	90.8±2.55	39.8 ± 1.7

mpound structure and the calculated solubility parameters with component group contributions (group contributions andbook[15].

Compound	Group	Quantity	F_{di} $J^{0.5}\cdot cm^{1.5}/mol$	F_{pi} $J^{0.5}\cdot cm^{1.5}/mol$	E_{hi} J/mol	V_i cm^3/mol	V cm^3/mol	δ_d $MPa^{0.5}$	δ_p $MPa^{0.5}$
Ibuprofen 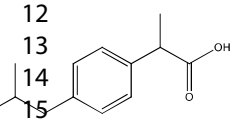		1	1270	110	0	-	193.94	18.97	2.24
	$CH_{aromatic}$	4	-	-	-	13.42			
	$C_{aromatic}$	2	-	-	-	7.42			
	$-CH_3$	3	420	0	0	21.55			
	$-CH_2-$	1	270	0	0	15.55			
	>CH–	2	80	0	0	9.56			
	Ring	1	190	0	0	-			
	–COOH	1	530	420	7000	26.1			
Isonicotinamide 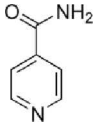	–NH2	1	280	0	8400	17	107.80	15.31	10.30
	–CO–	1	290	770	2000	17.3			
	Ring	1	190	0	0	-			
	=N-	1	20	800	5000	12.6			
	=CH–	4	200	0	0	13.18			
	=C<	1	70	0	0	8.18			
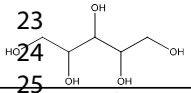	–OH	5	210	500	20000	12.45	122.03	15.00	9.16
	$-CH_2-$	2	270	0	0	15.55			
	>CH–	3	80	0	0	9.56			
Isonicotinamide equimolar cocrystal 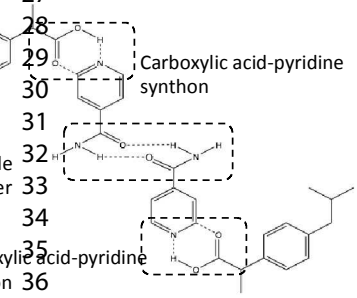 Carboxylic acid-pyridine synthon		2	1270	110	0	-	603.48	17.66	2.79
	$CH_{aromatic}$	8	-	-	-	13.42			
	$C_{aromatic}$	4	-	-	-	7.42			
	$-CH_3$	6	420	0	0	21.55			
	$-CH_2-$	2	270	0	0	15.55			
	>CH–	4	80	0	0	9.56			
	–COOH	2	530	420	7000	26.1			
	–NH2	2	280	0	8400	17			
	–CO–	2	290	770	2000	17.3			
	Ring	4	190	0	0	-			
	=N-	2	20	800	5000	12.6			
	=CH–	8	200	0	0	13.18			
	=C<	2	70	0	0	8.18			

Table 5 The molecular weights, true densities and melting temperatures of each individual compound used in the Flory-Huggins calculations. The melting temperature shown here represents the mean±SD of three replicates. Note that the melting temperature of Isonicotinamide was determined at a heating rate of 200°C/min to minimise influenced by sublimation.

Compound	M_w g/mol	ρ* g/cm^3	$T_{m\ (onset)}$ °C	$T_{m\ (peak)}$ °C	$T_{m(end)}$ °C	ΔH J/g
Ibuprofen	206.30	1.08	75.37±0.22	76.42±0.06	78.86±0.08	123.87±4.08
Isonicotinamide	122.12	1.34	155.37±0.45	162.58±0.97	169.79±1.62	199.21±9.80
Reference cocrystal	656.48	1.18	120.21±0.26	120.73±0.04	120.96±0.06	128.42±1.91
Xylitol	152.15	1.52	93.95±0.31	95.00±0.13	95.32±0.14	229.36±10.64

*The RSD for true density in the above measurements were all less than 0.07.

Figure legends

Figure 1 Schematic illustration of cocrystallisation mechanism, inside the extruder barrel, from a non-complementary carrier excipient.

Figure 2 DSC thermograms of (a) xylitol/Ibu mixtures obtained using a heating rate of 1°C/min; (b) IsoNA/xylitol mixtures obtained using a heating rate of 200°C/min; and (c) reference cocrystal/xylitol mixtures obtained using a heating rate of 1°C/min with various compositions.

Figure 3 The linear fit of the F-H interaction parameter χ and 1/T in Xylitol systems: (A) Ibu-Xylitol; (B) Isonicotinamide-Xylitol; and (C) equimolar cocrystal-Xylitol blends, respectively.

Figure 4 A plot of $\Delta G_{mix}/RT$ versus composition for (a) Ibu/xylitol, (b) IsoNA/xylitol and (c) reference cocrystal/xylitol mixtures, respectively, at various temperatures: ■ 80°C; ▲ 92°C; ● 95°C; ✶ 100°C; ◆ 110°C; + 115°C and, ▬ 120°C.

Figure 5 Liquid-solid phase transition diagrams for (a) xylitol/ibuprofen, (b) IsoNA/xylitol and (c) ref-cocrystal/xylitol mixtures, respectively. The solid diamonds represent the average χ determined from (n=3) replicate melting depression experiments, the dashed is the predicted solid-liquid line; the crosses give the F-H spinodal decomposition curve; and the solid triangle represents the critical solution temperature.

Figure 6 Overlain T-Φ spinodal lines for (from top down): cocrystal/xylitol, IsoNA/xylitol and, ibuprofen/xylitol systems, respectively. The arrows indicate regions in which respective phase behaviour (miscibility or separation) would occur based on the critical temperature predictions. It is clear that for the studied ternary system, an ideal HME processing window that meets all hypothesised criteria does not exist.

Figure 7 Calculated cocrystal yield from the melt-extruded suspensions. The pattern of the column represents the screw configuration profile: (blue) full-conveying profile SCP1, (green) intermediate intensity mixing profile SCP2, and (red) high intensity mixing profile SCP3, respectively. The label at the outer end of each column is the calculated average yield in percentage from 5 replicates. Note the columns are grouped according to the melting zone temperature setting.

Figure 8 Arrangement of: (a) forward conveying regions; (b) kneading regions used in SCP 2; (c) kneading region with two half-a-block-long 0° dispersive mixing sections in SCP 3 and; (d) consecutive neutral kneading sections in SCP 3.

Figure 9 Illustrative sketches showing the distribution and dispersion of materials in the staggering kneading region of an intermeshing modular twin-screw extruder: (a) distributive mixing caused by forcing material to flow around the kneading discs of a 90/4/10 block; (b) dispersive mixing flow of a 60/4/10 block caused by forcing material to flow through the narrow gap between the top of the shearing disc tip and the interior wall of extruder barrel.

Table captions

Table 1 Temperature profile settings TP1~TP5 designed to provide different thermodynamic environment for various degrees of mixing among raw ingredients.

Table 2 Specification of the screw configuration profile on one assembly shaft arranged from underneath the feed throat to the discharge end.

Table 3 Nomenclature and process conditions for the hot-melt extruded 1:1 Ibu-IsoNA cocrystal suspensions. Note that Ibu and IsoNA were premixed at a 1:1 molar ratio, whereas the weight fraction of xylitol in the ternary mixture was 50wt% for all extruded formulations.

Table 4 Compound structure and the calculated solubility parameters with component group contributions (group contributions obtained from Polymer Handbook[15].

Table 5 The molecular weights, true densities and melting temperatures of each individual compound used in the Flory-Huggins calculations. The melting temperature shown here represents the mean±SD of three replicates. Note that the melting temperature of Isonicotinamide was determined at a heating rate of 200°C/min to minimise influenced by sublimation.

Reference:

(1) Li, S.; Yu, T.; Tian, Y.; McCoy, C. P.; Jones, D. S.; Andrews, G. P. Mechanochemical Synthesis of Pharmaceutical Cocrystal Suspensions via Hot Melt Extrusion: Feasibility Studies and Physicochemical Characterization. *Mol. Pharm.* **2016**, *13* (9), 3054–3068.

(2) Bond, M.; Dunning, N. Xylitol. In *Sweeteners and Sugar Alternatives in Food Technology*; Blackwell Publishing Ltd, 2006; pp 295–328.

(3) Eddleston, M. D.; Patel, B.; Day, G. M.; Jones, W. Cocrystallization by Freeze-Drying: Preparation of Novel Multicomponent Crystal Forms. *Cryst. Growth Des.* **2013**, *13* (10), 4599–4606.

(4) Shan, N.; Toda, F.; Jones, W. Mechanochemistry and Co-Crystal Formation: Effect of Solvent on Reaction Kinetics. *Chem. Commun.* **2002**, No. 20, 2372–2373.

(5) Dhumal, R.; Kelly, A.; York, P.; Coates, P.; Paradkar, A. Cocrystalization and Simultaneous Agglomeration Using Hot Melt Extrusion. *Pharm. Res.* **2010**, *27* (12), 2725–2733.

(6) Rauwendaal, C. 10. Twin Screw Extruders. In *Polymer Extrusion*; Hanser: Munich, 2001; Vol. Revised 4t, pp 576–633.

(7) Giles, H. F.; Wagner, J. R.; Mount, E. M. *Extrusion: The Definitive Processing Guide and Handbook*; William Andrew Pub: Norwich, NY, 2005.

(8) Hancock, B. C.; York, P.; Rowe, R. C. The Use of Solubility Parameters in Pharmaceutical Dosage Form Design. *Int. J. Pharm.* **1997**, *148* (1), 1–21.

(9) Greenhalgh, D. J.; Williams, A. C.; Timmins, P.; York, P. Solubility Parameters as Predictors of Miscibility in Solid Dispersions. *J. Pharm. Sci.* **1999**, *88* (11), 1182–1190.

(10) Forster, A.; Hempenstall, J.; Tucker, I.; Rades, T. Selection of Excipients for Melt Extrusion with Two Poorly Water-Soluble Drugs by Solubility Parameter Calculation and Thermal Analysis. *Int. J. Pharm.* **2001**, *226* (1–2), 147–161.

(11) Mohammad, M. A.; Alhalaweh, A.; Velaga, S. P. Hansen Solubility Parameters as a Tool to Predict Cocrystal Formation. *Int. J. Pharm.* **2011**, *407*, 63–71.

(12) Fukte, S. R.; Wagh, M. P.; Rawat, S. Coformer Selection: An Important Tool in Cocrystal Formation. *Int. J. Pharm. Pharm. Sci.* **2014**, *6* (7), 9–14.

(13) Fedors, R. F. A Method for Estimating Both the Solubility Parameters and Molar Volumes of Liquids. *Polym. Eng. Sci.* **1974**, *14* (2), 147–154.

(14) Van Krevelen, D. W.; Hoftyzer, P. J. *Properties of Polymers, Their Estimation and Correlation with Chemical Structure*; Elsevier Scientific Pub. Co.: Amsterdam and New York, 1976; Vol. 2nd.

(15) Grulke, E. A. Solubility Parameter Values. In *Polymer Handbook*; Brandrup, J., Immergut, E. H., Grulke, E. A., Eds.; John Wiley & Sons, Inc.: New York. Chichester. Weinheim. Brisbane. Singapore. Toronto., 1999; Vol. Fourth, p VII/675-VII/687.

(16) Donnelly, C.; Tian, Y.; Potter, C.; Jones, D. S.; Andrews, G. P. Probing the Effects of Experimental Conditions on the Character of Drug-Polymer Phase Diagrams Constructed Using Flory-Huggins Theory. *Pharm. Res.* **2015**, *32* (1), 167–179.

(17) Padrela, L.; de Azevedo, E. G.; Velaga, S. P. Powder X-Ray Diffraction Method for the Quantification of Cocrystals in the Crystallization Mixture . *Drug Dev. Ind. Pharm.* **2012**, *38* (8), 923–929.

(18) Guidelines, I. C. H. Internation Conference on Harmonization (ICH) Harmonized Tripartite Guideline, Note for Guidance on Validation of Analytical Procedures: Methodology. ICH Steering Committee 1996.

(19) Flory, P. J. Thermodynamics of High Polymer Solutions . *J. Chem. Phys.* **1941**, *9* (8), 660.

(20) Flory, P. J. Thermodynamics of High Polymer Solutions. *J. Chem. Phys.* **1942**, *10* (51).

(21) Huggins, M. L. Solutions of Long Chain Compounds . *J. Chem. Phys.* **1941**, *9* (5), 440.

(22) Huggins, M. L. Some Properties of Solutions of Long-Chain Compounds. *J. Phys. Chem.* **1942**, *46* (1), 151–158.

(23) Lin, D.; Huang, Y. A Thermal Analysis Method to Predict the Complete Phase Diagram of Drug-Polymer Solid Dispersions. *Int. J. Pharm.* **2010**, *399*, 109–115.

(24) Nishi, T.; Wang, T. T. Melting Point Depression and Kinetic Effects of Cooling on Crystallization in Poly(vinylidene Fluoride)-Poly(methyl Methacrylate) Mixtures. *Macromolecules* **1975**, *8* (6), 909–915.

(25) Jo, W. H.; Kwan, I. H. Equation of State Theory for Melting Point Depression in Miscible Polymer Blends. *Macromolecules* **1991**, *24* (11), 3368–3372.

(26) Marsac, P. J.; Li, T.; Taylor, L. S. Estimation of Drug-Polymer Miscibility and Solubility in Amorphous Solid Dispersions Using Experimentally Determined Interaction Parameters. *Pharm. Res.* **2009**, *26* (1), 139–151.

(27) Paudel, A.; Van Humbeeck, J.; Van Den Mooter, G. Theoretical and Experimental Investigation on the Solid Solubility and Miscibility of Naproxen in Poly(vinylpyrrolidone). *Mol. Pharm.* **2010**, *7* (4), 1133–1148.

(28) Zhao, Y. Y.; Inbar, P.; Chokshi, H.; Malick, A. W.; Choi, D. S. Prediction of the Thermal Phase Diagram of Amorphous Solid Dispersions by Flory-Huggins Theory. *J. Pharm. Sci.* **2011**, *100* (8), 3196–3207.

(29) Tian, Y. W.; Booth, J.; Meehan, E.; Jones, D. S.; Li, S.; Andrews, G. P. Construction of Drug–Polymer Thermodynamic Phase Diagrams Using Flory–Huggins Interaction Theory: Identifying the Relevance of Temperature and Drug Weight Fraction to Phase Separation within Solid Dispersions. *Mol. Pharm.* **2013**, *10* (1), 236–248.

(30) Tian, Y.; Caron, V.; Jones, D. S.; Healy, A.-M.; Andrews, G. P. Using Flory-Huggins Phase Diagrams as a Pre-Formulation Tool for the Production of Amorphous Solid Dispersions: A Comparison between Hot-Melt Extrusion and Spray Drying. *J. Pharm. Pharmacol.* **2014**, *66* (2), 256–274.

(31) Li, S.; Tian, Y.; Jones, D. S.; Andrews, G. P. Optimising Drug Solubilisation in Amorphous Polymer Dispersions: Rational Selection of Hot-Melt Extrusion Processing Parameters. *AAPS PharmSciTech* **2016**, *17* (1), 200–213.

(32) Rubinstein, M.; Colby, R. *Polymer Physics*; Oxford University Press Inc.: New York, 2003.

(33) Almarsson, O.; Zaworotko, M. J. Crystal Engineering of the Composition of Pharmaceutical Phases. Do Pharmaceutical Co-Crystals Represent a New Path to Improved Medicines? . *Chem. Commun.* **2004**, *7* (17), 1889–1896.

(34) Basavoju, S.; Boström, D.; Velaga, S. Indomethacin–Saccharin Cocrystal: Design, Synthesis and Preliminary Pharmaceutical Characterization. *Pharmaceutical Research*. Springer Netherlands **2008**, *25* (3), pp 530–541.

(35) Alhalaweh, A.; Velaga, S. P. Formation of Cocrystals from Stoichiometric Solutions of Incongruently Saturating Systems by Spray Drying. *Cryst. Growth Des.* **2010**, *10* (8), 3302–3305.

(36) Prasad, R. V.; Rakesh, M. G.; Jyotsna, R. M.; Mangesh, T.; Anita, P. S.; Mayur, P. K. Pharmaceutical Cocrystallization: A Review. *Int. J. Pharm. Chem. Sci.* **2012**, *1* (3), 725–736.

(37) Almarsson, Ö.; Peterson, M. L.; Zaworotko, M. J. The A to Z of Pharmaceutical Cocrystals: A Decade of Fast Moving New Science and Patents. *Pharm. Pat. Anal.*

2012, *1* (3), 313–327.

(38) FriŠčić, T.; Trask, A. V; Jones, W.; Motherwell, W. D. S. Screening for Inclusion Compounds and Systematic Construction of Three-Component Solids by Liquid-Assisted Grinding. *Angew. Chemie* **2006**, *118* (45), 7708–7712.

(39) FriŠčić, T.; Fabian, L.; Burley, J. C.; Jones, W.; Motherwell, W. D. S. Exploring Cocrystal-Cocrystal Reactivity via Liquid-Assisted Grinding: Assembling of Racemic and Dismantling of Enantiomeric Cocrystals . *Chem. Commun.* **2006**, *28* (48), 5009–5011.

(40) FriŠčić, T.; Childs, S. L.; Rizvi, S. A. A.; Jones, W. The Role of Solvent in Mechanochemical and Sonochemical Cocrystal Formation: A Solubility-Based Approach for Predicting Cocrystallisationoutcome. *Cryst. Growth Des.* **2009**, *11* (3), 418–426.

(41) Lin, H.-L.; Hsu, P.-C.; Lin, S.-Y. Theophylline–citric Acid Co-Crystals Easily Induced by DSC–FTIR Microspectroscopy or Different Storage Conditions. *Asian J. Pharm. Sci.* **2013**, *8* (1), 19–27.

(42) Shevchenko, A.; Miroshnyk, I.; Pietilä, L.-O.; Haarala, J.; Salmia, J.; Sinervo, K.; Mirza, S.; van Veen, B.; Kolehmainen, E.; Yliruusi, J. Diversity in Itraconazole Cocrystals with Aliphatic Dicarboxylic Acids of Varying Chain Length . *Cryst. Growth Des.* **2013**, *13* (11), 4877–4884.

(43) Zhang, G. G. Z.; Henry, R. F.; Borchardt, T. B.; Lou, X. Efficient Co-Crystal Screening Using Solution-Mediated Phase Transformation. *J. Pharm. Sci.* **2007**, *96* (5), 990–995.

(44) Etter, M. C.; Reutzel, S. M.; Choo, C. G. Self-Organization of Adenine and Thymine in the Solid State. *J. Am. Chem. Soc.* **1993**, *115* (10), 4411–4412.

(45) Trask, A. V.; Jones, W. Crystal Engineering of Organic Cocrystals by the Solid-State Grinding Approach. *Topics in Current Chemistry*. **2005**, *254*, pp 41–70.

(46) Liu, X.; Lu, M.; Guo, Z.; Huang, L.; Feng, X.; Wu, C. Improving the Chemical Stability of Amorphous Solid Dispersion with Cocrystal Technique by Hot Melt Extrusion . *Pharm. Res.* **2012**, *29* (3), 806–817.

(47) Seefeldt, K.; Miller, J.; Alvarez-Núñez, F.; Rodríguez-Hornedo, N. Crystallization Pathways and Kinetics of Carbamazepine?nicotinamide Cocrystals from the Amorphous State by in Situ Thermomicroscopy, Spectroscopy, and Calorimetry Studies. *J. Pharm. Sci.* **2007**, *96* (5), 1147–1158.

(48) Hansen, C. M. *Hansen Solubility Parameters: A User's Handbook* ; CRC Press: Boca Raton, 2007; Vol. Second.

(49) Abbott, S.; Hansen, C. M. *Hansen Solubility Parameters in Practice*; Hansen-Solubility.com, 2008.

(50) Yang, M.; Wang, P.; Gogos, C. G. A New Systematic Methodology to Determine Drug's Solubility in Polymer. In *ANTEC*; 2011.

(51) Aakeröy, C. B.; Beatty, A. M.; Helfrich, B. A.; Nieuwenhuyzen, M. Do Polymorphic Compounds Make Good Cocrystallizing Agents? A Structural Case Study That Demonstrates the Importance of Synthon Flexibility. *Cryst. Growth Des.* **2003**, *3* (2), 159–165.

(52) Li, J.; Bourne, S. a; Caira, M. R. New Polymorphs of Isonicotinamide and Nicotinamide. *Chem. Commun.* **2011**, *47* (5), 1530–1532.

(53) Berry, D. J.; Seaton, C. C.; Clegg, W.; Harrington, R. W.; Coles, S. J.; Horton, P. N.; Hursthouse, M. B.; Storey, R.; Jones, W.; Friscic, T.; Blagden, N. Applying Hot-Stage Microscopy to Co-Crystal Screening: A Study of Nicotinamide with Seven Active Pharmaceutical Ingredients . - *Cryst. Growth Des.* **2008**, No. 5, 1697–1712.

(54) Rauwendaal, C. *Mixing in Polymer Processing*; M. Dekker: New York, 1991; Vol. 23.

(55) Nakayama, Y.; Takeda, E.; Shigeishi, T.; Tomiyama, H.; Kajiwara, T. Melt-Mixing by Novel Pitched-Tip Kneading Disks in a Co-Rotating Twin-Screw Extruder. *Chem. Eng. Sci.* **2011**, *66* (1), 103–110.

(56) Yang, H.-H.; Manas-Zloczower, I. Flow Field Analysis of the Kneading Disc Region in a Co-Rotating Twin Screw Extruder. *Polym. Eng. Sci.* **1992**, *32* (19), 1411–1417.

(57) Kalyon, D. M.; Sangani, H. N. An Experimental Study of Distributive Mixing in Fully Intermeshing, Co-Rotating Twin Screw Extruders. *Polym. Eng. Sci.* **1989**, *29* (15), 1018–1026.

(58) Sarhangi Fard, A.; Anderson, P. D. Simulation of Distributive Mixing inside Mixing Elements of Co-Rotating Twin-Screw Extruders. *Comput. Fluids* **2013**.

(59) Wang, W.; Manas-Zloczower, I. Analysis of Dispersive and Distributive Mixing In Terms of Minor Component Size and Spatial Distributions in Continuous Polymer Processing Equipment. 2000.

(60) Paul, E. L.; Atiemo-Obeng, V.; Kresta, S. M. *Handbook of Industrial Mixing: Science and Practice*; Jon Wiley & Sons, Inc.: New Jersy, 2004.

(61) Manas-Zloczower, I. *Mixing and Compounding of Polymers: Theory and Practice*; Hanser, 2009.

(62) Gogos, C. G.; Liu, H.; Wang, P. Laminar Dispersive and Distributive Mixing with Dissolution and Applications to Hot-Melt Extrusion. In *Hot-Melt Extrusion: Pharmaceutical Applications*; Douroumis, D., Ed.; John Wiley & Sons, Ltd, 2012; pp 261–284.

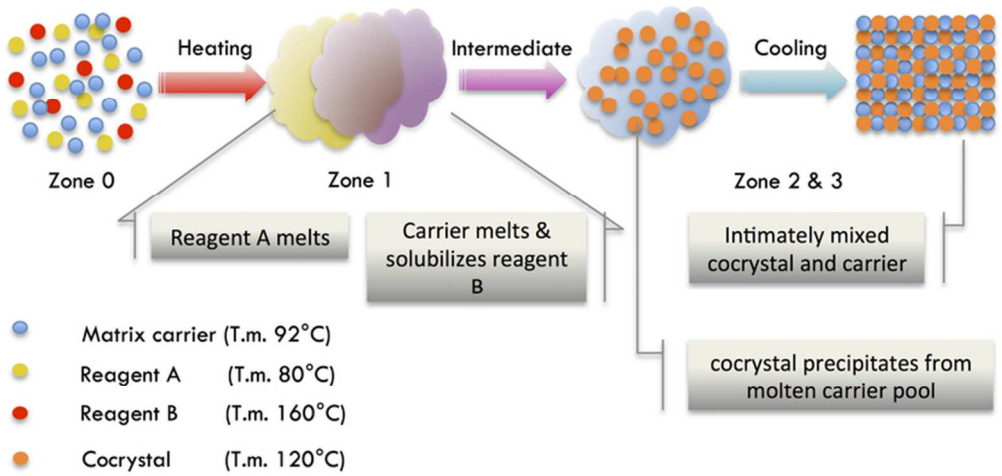

Figure 1 Schematic illustration of cocrystallisation mechanism, inside the extruder barrel, from a non-complementary carrier excipient.

70x33mm (300 x 300 DPI)

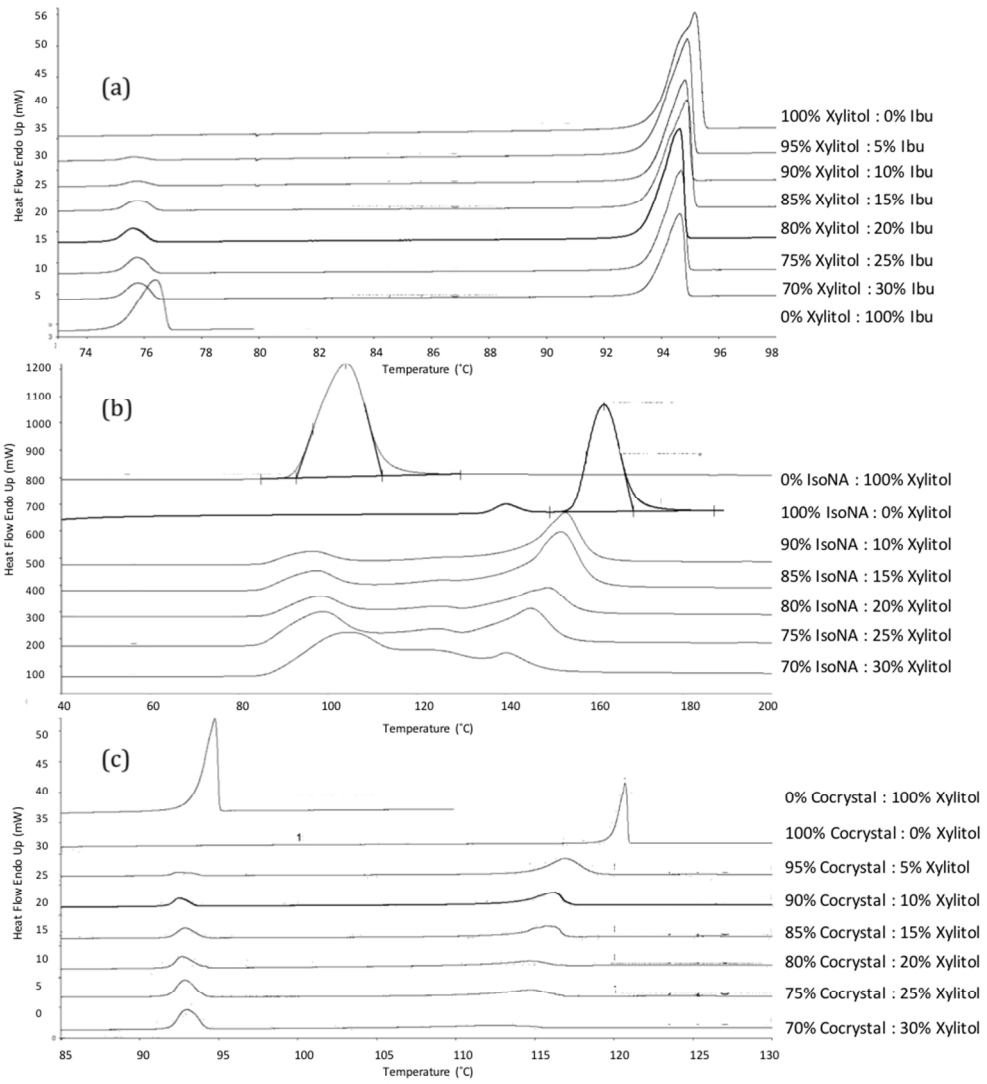

Figure 2 DSC thermograms of (a) xylitol/Ibu mixtures obtained using a heating rate of 1°C/min; (b) IsoNA/xylitol mixtures obtained using a heating rate of 200°C/min; and (c) reference cocrystal/xylitol mixtures obtained using a heating rate of 1°C/min with various compositions.

175x190mm (150 x 150 DPI)

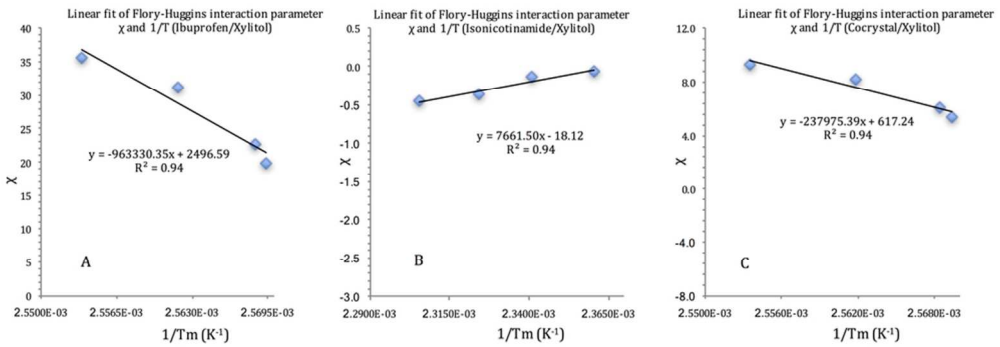

Figure 3 The linear fit of the F-H interaction parameter χ and 1/T in Xylitol systems: (A) Ibu-Xylitol; (B) Isonicotinamide-Xylitol; and (C) equimolar cocrystal-Xylitol blends, respectively.

84x29mm (300 x 300 DPI)

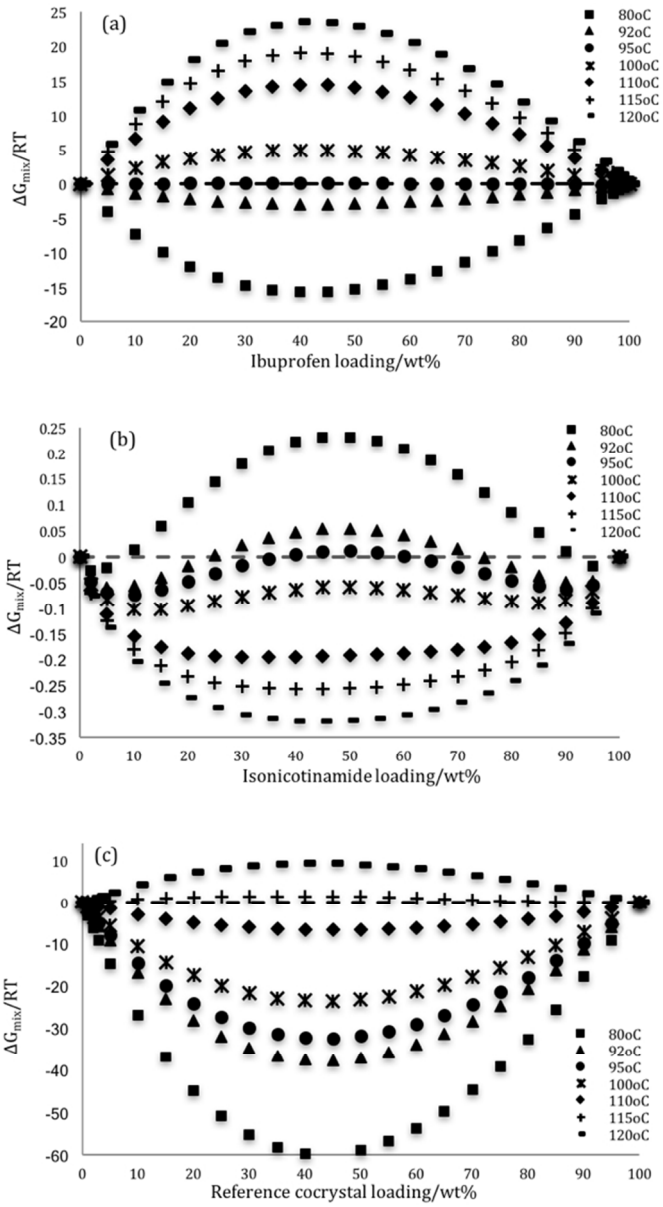

Figure 4 A plot of ΔGmix/RT versus composition for (a) Ibu/xylitol, (b) IsoNA/xylitol and (c) reference cocrystal/xylitol mixtures, respectively, at various temperatures: 80°C; 92°C; 95°C; 100°C; 110°C; 115°C and, 120°C, respectively.

107x190mm (150 x 150 DPI)

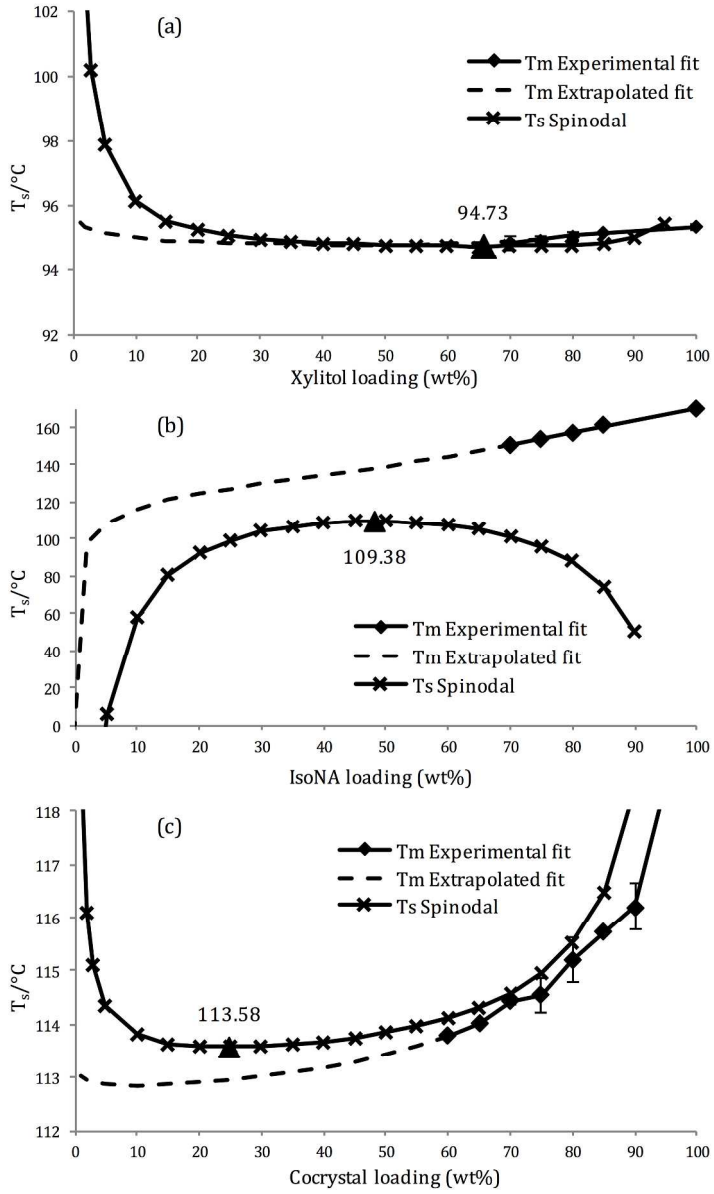

Figure 5 Liquid-solid phase transition diagrams for (a) xylitol/ibuprofen, (b) IsoNA/xylitol and (c) ref-cocrystal/xylitol mixtures, respectively. The solid diamonds represent the average χ determined from (n=3) replicate melting depression experiments, the dashed is the predicted solid-liquid line; the crosses give the F-H spinodal decomposition curve; and the solid triangle represents the critical solution temperature.

209x346mm (300 x 300 DPI)

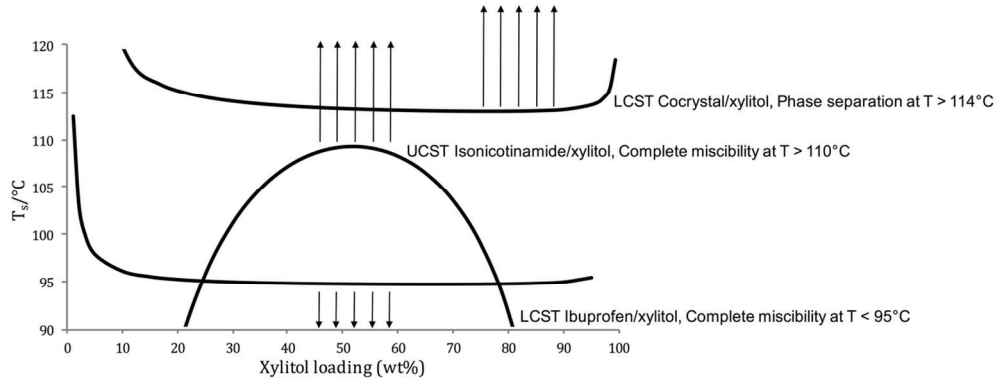

Figure 6 Overlain T-Φ spinodal lines for (from top down): cocrystal/xylitol, IsoNA/xylitol and, ibuprofen/xylitol systems, respectively. The arrows indicate regions in which respective phase behaviour (miscibility or separation) would occur based on the critical temperature predictions. It is clear that for the studied ternary system, an ideal HME processing window that meets all hypothesised criteria does not exist.

118x45mm (300 x 300 DPI)

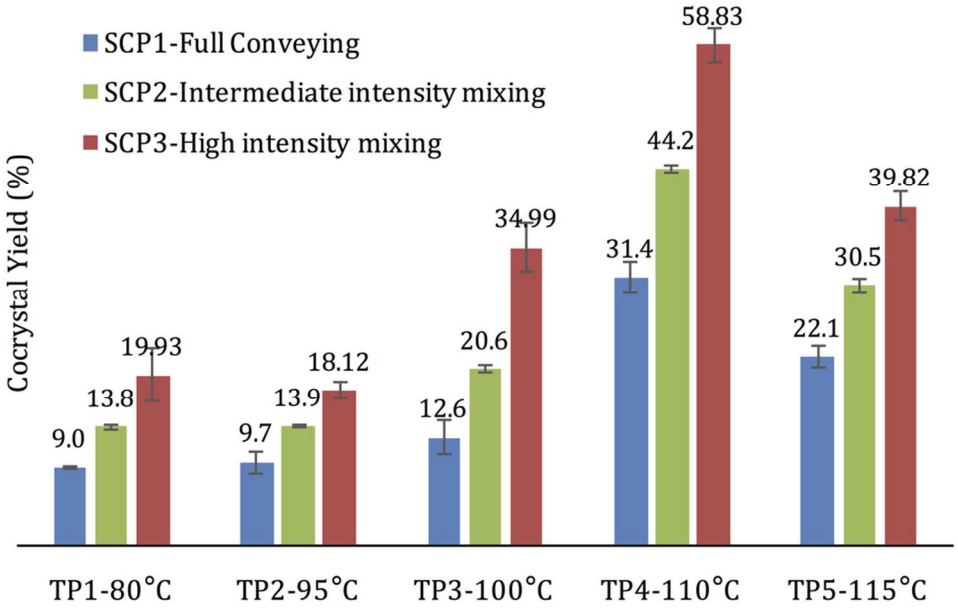

Figure 7 Calculated cocrystal yield from the melt-extruded suspensions. The pattern of the column represents the screw configuration profile: (blue) full-conveying profile SCP1, (green) intermediate intensity mixing profile SCP2, and (red) high intensity mixing profile SCP3, respectively. The label at the outer end of each column is the calculated average yield in percentage from 5 replicates. Note the columns are grouped according to the melting zone temperature setting.

93x59mm (300 x 300 DPI)

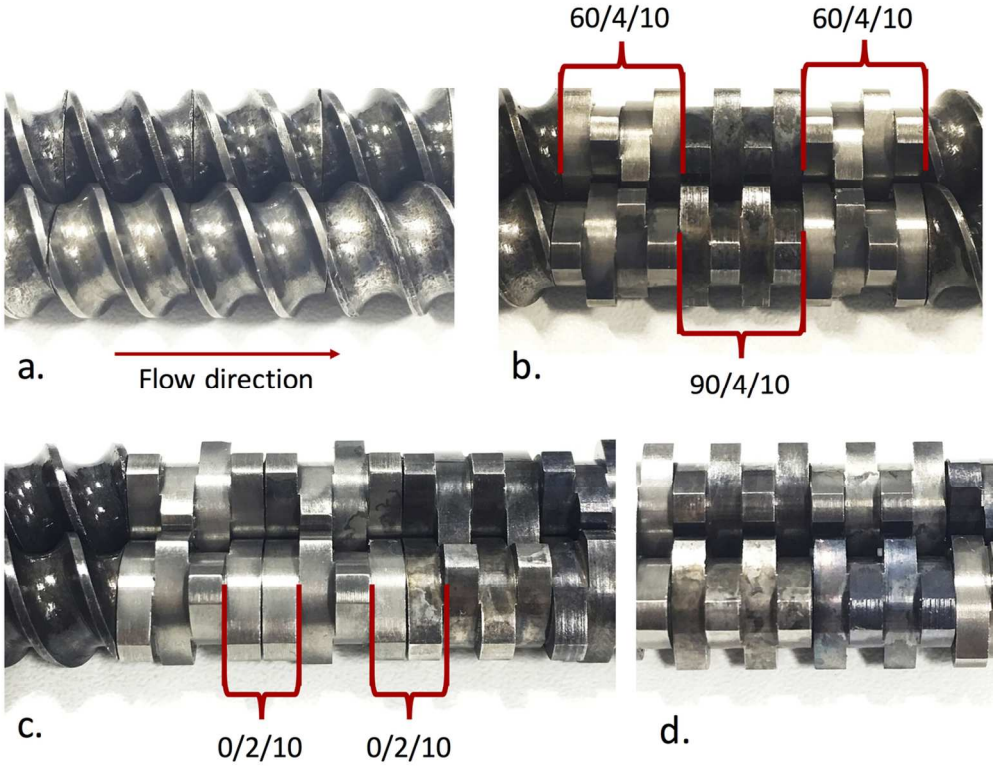

Figure 8 Arrangement of: (a) forward conveying regions; (b) kneading regions used in SCP 2; (c) kneading region with two half-a-block-long 0° dispersive mixing sections in SCP 3 and; (d) consecutive neutral kneading sections in SCP 3.

116x93mm (300 x 300 DPI)

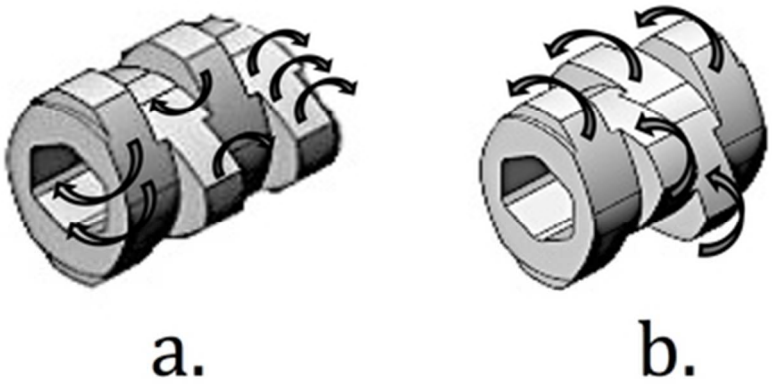

Figure 9 Illustrative sketches showing the distribution and dispersion of materials in the staggering kneading region of an intermeshing modular twin-screw extruder: (a) distributive mixing caused by forcing material to flow around the kneading discs of a 90/4/10 block; (b) dispersive mixing flow of a 60/4/10 block caused by forcing material to flow through the narrow gap between the top of the shearing disc tip and the interior wall of extruder barrel.

35x18mm (300 x 300 DPI)

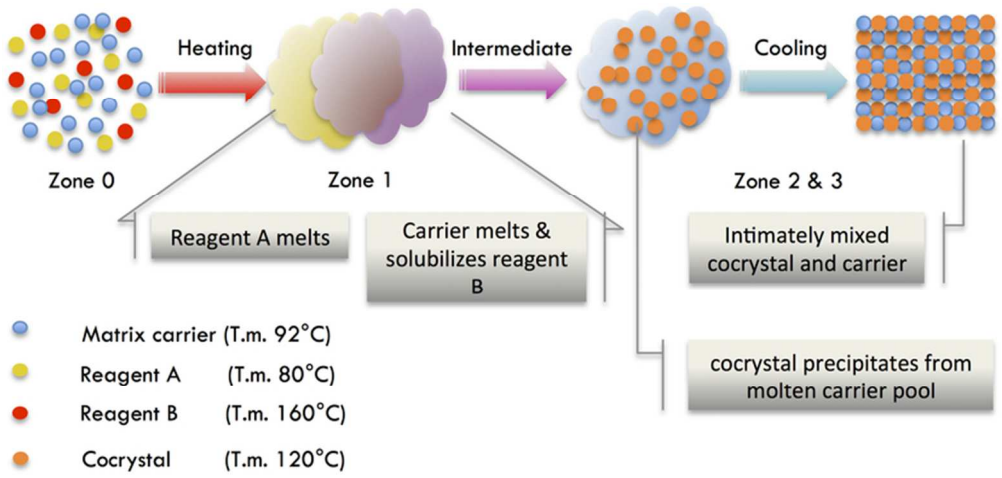

Table of Contents Graphic

70x33mm (300 x 300 DPI)